

Observation of anti-magnetic rotations in ^{104}Pd

N. Rather^a, S. Roy^{b,*}, P. Datta^c, S. Chattopadhyay^a, A. Gowsami^a, S. Nag^d, R. Palit^b, S. Pal^b, S. Saha^b, J. Sethi^b, T. Trivedi^b, H. C. Jain^b

^a*Saha Institute of Nuclear Physics, 1/AF Bidhannagar, Kolkata 700 064, India*

^b*Tata Institute of Fundamental Research, Homi Bhabha Road, Mumbai 400 005, India*

^c*Ananda Mohan College, 102/1 Raja Rammohan Roy Sarani, Kolkata 700 009, India*

^d*Indian Institute of Technology, Kharagpur-721302, West Bengal, India*

Abstract

The electric quadrupole transition rates for the high spin yrast states of ^{104}Pd have been measured by using the DSAM technique. These values decrease with the increase of angular momentum which is a signature of anti-magnetic rotation. A numerical calculation based on semi-classical particle plus rotor model for anti-magnetic rotation gives a good description of the experimental routhian and the transition rates. This is the first observation of AMR in a nucleus other than Cadmium.

Anti-magnetic rotation (AMR) is a novel mechanism for the generation of high angular momentum states in atomic nuclei and was first proposed by S. Frauendorf [1, 2]. This excitation mode derives its origin from the shears mechanism which is responsible for the origin of M1 bands observed in $A \sim 180$, 130 and 100 regions [3, 4]. In the semi-classical picture of shears mechanism, the total angular momentum is generated by the angular momenta of the valence protons and neutrons and the single particle configuration is such that it allows the perpendicular coupling of these two angular momentum vectors. Thus, at the band head, the angle between them (shears angle, θ) is 90° and the higher angular momentum states of the band originate from the gradual closing of the two angular momentum vectors around the total which resembles the closing of a pair of shears. AMR is a special case of symmetric multi-shears configuration, which is formed by the two angular momentum vectors of a pair of deformation - aligned protons (neutrons) in time reversed orbits ($\mathbf{j}_h^{(1)}$ and $\mathbf{j}_h^{(2)}$) and the angular momentum vector of multiple rotation - aligned neutrons (protons) (\mathbf{j}_p). This structure is symmetric because the shears angle (θ) between $\mathbf{j}_h^{(1)} - \mathbf{j}_p$ and $\mathbf{j}_h^{(2)} - \mathbf{j}_p$ is the same. Thus, the higher angular momentum states, in case of AMR, are generated by the simultaneous closure of the multi-shear around (\mathbf{j}_p) and is given by

$$I_{sh} = j_p + 2j_h \cos\theta \quad (1)$$

The symmetry of this shears structure implies that the perpendicular components of the magnetic moment for the two shears cancel each other. For this reason the dipole transition rate vanishes for AMR. The cancellation of the magnetic moment has induced the

*Corresponding author

Email address: santoshroy@gmail.com (S. Roy)

Preprint submitted to Elsevier

January 21, 2020

name Anti-magnetic Rotation due to its similarity with anti-ferromagnetism where the dipole moment of one sub-lattice is in opposite direction to the other half leading to the absence of the net magnetic moment. However, as the $R_z(\pi)$ symmetry is retained, the rotational structure decays by weak electric quadrupole (E2) transitions. This transition rate is given by [4]

$$B(E2) = \frac{15}{32\pi}(eQ)_{eff}^2 \sin^4\theta \quad (2)$$

where Q_{eff} is the effective quadrupole moment of the core (rotor). Thus, the B(E2) rates are expected to drop with increasing angular momentum for AMR.

This mode was first experimentally observed in ^{106}Cd by Simons *et al.* [5] and subsequently in ^{108}Cd by P. Datta *et al.* [6]. In both the cases the AMR was built on $\pi(g_{9/2})^{-2} \otimes \nu[(g_{7/2}/d_{5/2})^2(h_{11/2})^2]$ configuration and the band heads were found to be at $18\hbar$ and $16\hbar$ for ^{106}Cd and ^{108}Cd , respectively. The AMR mechanism accounted for an angular momentum increase of $8\hbar$ which corresponded to the complete alignment of the two proton holes and the B(E2) rates were found to decrease continuously in this spin domain.

The interplay between collective and the anti-magnetic rotations was first reported by Roy *et. al* [7] in ^{110}Cd where the AMR band was built on $\pi(g_{9/2})^{-2} \otimes \nu(h_{11/2})^2$ configuration. This interplay was found to span over an angular momentum range of $18\hbar$ of which $10\hbar$ was due to collective rotation. In this work, a semi-classical particle rotor model calculation could successfully reproduce the observed alignment feature. The parameters of the model were determined from the observed systematics in $^{106,108}\text{Cd}$. The effect of the interplay was concluded from the slower fall of B(E2) rates in ^{110}Cd as compared to the pure AMR bands in $^{106,108}\text{Cd}$ [7]. Such interplay was later reported in $^{105,107}\text{Cd}$ [8, 9]. Apart from Cd isotopes mentioned above, experimental investigations of ^{100}Pd [10], ^{101}Pd [11] and ^{144}Dy [12] have indicated the possibility of existence of AMR bands in these nuclei. However, due to the absence of lifetime measurements, the bands of these nuclei could not be identified with AMR. The present work reports the lifetime measurements of the high spin yrast states of ^{104}Pd and establishes AMR for the first time in a nucleus which is not an isotope of Cadmium.

In order to populate the high spin states of ^{104}Pd , the ^{13}C beam of 63 MeV delivered by 14-UD Pelletron at TIFR was bombarded on 1 mg/cm² enriched ^{96}Zr target. The target had a ^{206}Pb backing of 9 mg/cm² thickness. The de-exciting γ rays were detected using the Indian National Gamma Array (INGA) [13] which consisted of 18 Compton suppressed clover detectors. Two and higher fold coincidence data were recorded by fast digital data acquisition system based on Pixie-16 modules of XIA LLC [14]. The corresponding time stamped data were sorted in a γ - γ - γ Cube using the Multi-PARAMeter time stamped based Coincidence Search program (MARCOS), developed at TIFR. The Cube was used to established the low lying levels of ^{104}Pd exhibiting no lineshapes with the help of the RADWARE program LEVIT8R [15]. It was also used to determine their relative intensities. An asymmetric 90° -vs-all γ - γ matrix was constructed by placing the γ -energy detected at 90° along one axis and the coincident γ -energy detected at any other angle along the other axis. The 90° projections of different γ -gates on this matrix were used to extend the level scheme to higher spins and to measure the corresponding relative intensities since the angle summed symmetric cube was not suitable for the extraction of intensities of the γ rays with lineshapes. The level scheme and the extracted intensities from the present work are in agreement with the earlier report[16]. The level scheme of

the yrast cascade of ^{104}Pd is shown in Fig. 1 where the widths of the transitions are proportional to their relative intensities.

The MARCOS was also used to construct two more angle dependant γ - γ asymmetric matrices for the angles 40° and 157° . These two matrices were used to extract the lineshapes for the levels above $I = 14\hbar$ of ^{104}Pd at the forward and the backward angles. The theoretical lineshapes were derived using the code LINESHAPE by Wells and Johnson [17]. A Monte Carlo simulation of the slowing down process of the recoiling nuclei in the target and the backing was used to generate the velocity profiles at the three angles of 40° , 90° and 157° . These profiles were obtained at a time interval of 0.001 ps for 5000 histories of energy losses at different depths of the target and its backing. The stopping power formula of Northcliffe and Schilling [18] with shell correction was used for calculating these energy losses. The energies and intensities of the γ -transitions were treated as the input parameters to the lineshape fits. The side feeding intensities were fixed to reproduce the observed intensity pattern along the yrast cascade shown in Fig. 1. The side feeding intensity to each level has been modelled as a cascade of five transitions with a moment of inertia which is comparable to that of the band of interest. The quadrupole moments of the side feeding sequence were allowed to vary which when combined with the moment of inertia gave an effective side feeding time for each level. For each observed lineshape, in-band and side-feeding lifetimes and the intensities of the contaminant peaks (if present), were allowed to vary. For each set of parameters, the simulated lineshapes were fitted to the experimental spectrum using χ^2 -minimization routine of MINUIT [19].

The topmost transition of 1468 keV ($26^+ \rightarrow 24^+$) was assumed to have 100% sidefeed. The other parameters were allowed to vary until the minimum χ^2 value was reached. This led to the estimation of the effective lifetime for the 26^+ level. For the 24^+ level decaying through 1365 keV transition, the effective lifetime of the 26^+ level and the side-feeding lifetime were considered as the input parameters. In this way, each lower level was added one by one and fitted until all of the observed lineshapes of the yrast cascade of ^{104}Pd were included into a global fit where only the in-band and the side-feeding lifetimes were allowed to vary. The uncertainties in the measurement were derived from the behaviour of the χ^2 fit in the vicinity of the minimum. This procedure of global fit was repeated at forward (40°) and backward (157°) angles. Thus, the final value for the level lifetime was obtained by taking average from the fits at the two angles. The corresponding uncertainty has been calculated as the average of the uncertainties for the two independent lifetime measurements for that level added in quadrature.

In the present analysis all the lineshapes were extracted from the 803 keV γ -gated spectrum. In this gate the lineshape of 927 keV transition ($16^+ \rightarrow 14^+$) was strongly contaminated by 926 keV transition ($6^+ \rightarrow 4^+$). However, it was found from the data that the γ -transitions below 10^+ state did not exhibit lineshapes. Thus, the 926 keV transition could be treated as a contaminant peak. The intensity of this stopped peak was estimated from the efficiency corrected areas of 556 ($2^+ \rightarrow 0^+$), 768 ($4^+ \rightarrow 2^+$) and 971 ($8^+ \rightarrow 6^+$) keV transitions in the 803 keV γ -gate. These areas were found to be equal within $\pm 1\%$. So a stopped peak at 926 keV with this averaged area was used to determine the true lineshape of 927 keV transition. The examples of the lineshape fits for the three top transitions in ^{104}Pd are shown in Fig. 2.

The B(E2) transition rates were extracted from the measured level lifetimes using the

formula [20]

$$B(E2) = \frac{0.0816}{E_\gamma^5 \times \tau} \quad (3)$$

where E_γ is the energy in MeV of a pure E2 transition, τ is the level lifetime in picoseconds and $B(E2)$ is in the units of $(eb)^2$. The extracted $B(E2)$ values are tabulated in Table I where the error bars on the values include the uncertainties on lifetime and intensity measurements added in quadrature. The $B(E2)$ values have been plotted as a function of angular momentum in Fig. 3(a) which show a monotonically falling behaviour. In addition, the values for the $\mathcal{J}^{(2)}/B(E2)$ ratio for levels $I^\pi = 16^+$ and above were found to be an order of magnitude larger than those for a well-deformed collective rotor and increased with spin. This is expected for an AMR band as the $B(E2)$ values are small and decrease with spin while the $\mathcal{J}^{(2)}$ remains nearly constant. The values of this ratio are also tabulated in Table I. Thus, the high spin levels of the yrast cascade of ^{104}Pd seem to originate due to anti-magnetic rotation.

In order to explore this possibility further, a numerical calculation based on the framework of semi-classical particle rotor model has been performed. This model has been successfully employed to describe the observed spectroscopic features of the AMR bands in Cd-isotopes [7, 21]. In this model, the energy $E(I)$ is given by :

$$E(I) = \frac{(\mathbf{I} - \mathbf{j}_\pi - \mathbf{j}_\nu)^2}{2\mathfrak{S}} + \frac{V_{\pi\nu}}{2} \left(\frac{3\cos^2\theta - 1}{2} \right) + \frac{V_{\pi\nu}}{2} \left(\frac{3\cos^2(-\theta) - 1}{2} \right) - \frac{V_{\pi\pi}}{n} \left(\frac{3\cos^2(2\theta) - 3}{2} \right) \quad (4)$$

where the first term represents the rotational contribution and \mathfrak{S} is the associated moment of inertia. The second and the third terms signify the repulsive interaction between the neutron particles and the proton holes and $V_{\pi\nu}$ is the interaction strength. The fourth term is the proton - proton (hole - hole) attractive interaction and has been assumed to be of the same form with the additional boundary condition that it vanishes for $\theta = 0^\circ$. This condition also implies that the attractive particle - particle interaction is absent. There is a scaling factor n between $V_{\pi\nu}$ and $V_{\pi\pi}$ and is determined by the actual number of particle - hole pairs for a single particle configuration. The systematic study of AMR in even - even Cd isotopes has indicated that the strength of the particle - hole and hole - hole interactions are 1.2 and 0.15 - 0.2 MeV, respectively [7]. Since ^{104}Pd is the immediate even - even neighbour of ^{106}Cd , it is therefore expected that the same interaction strength should be valid.

The angular momentum generated by the interplay between collective rotation and AMR can be calculated by imposing the energy minimization condition as a function of θ on Eq. (3), which gives:

$$I = aj + 2j \cos\theta + \frac{1.5\mathfrak{S}V_{\pi\nu} \cos\theta}{j} - \frac{6\mathfrak{S}V_{\pi\pi} \cos 2\theta \cos\theta}{nj} \quad (5)$$

or,

$$I = I_{sh} + \mathfrak{S}\omega_{sh} \quad (6)$$

where, $j = j_\pi$, $a = j_\nu/j_\pi$, I_{sh} is the sum of the first two terms of Eq. (5) and $\omega_{sh} = \left(\frac{dE_{sh}}{d\theta} \right) / \left(\frac{dI_{sh}}{d\theta} \right)$ which represents the frequency associated with the shears mechanism and is given by

$$\omega_{sh} = \frac{(1.5V_{\pi\nu}/j) \cos\theta - (6V_{\pi\pi}/nj) \cos 2\theta \cos\theta}{4} \quad (7)$$

Thus, in this model the total angular momentum is generated by the shears mechanism (I_{sh}) and the interplay between shears mechanism and collective rotation represented by $\Im\omega_{sh}$ in Eq. (6). The magnitude of \Im can be estimated from the equation

$$\Im\omega_{sh}|_{(\theta=0^\circ)} = I_{max} - I_{sh}^{max} \quad (8)$$

where I_{max} is the highest observed angular momentum state and I_{sh}^{max} is the maximum angular momentum generated by the full closure of the double shear. The rotational frequency ω is given by

$$\omega = \omega_{rot} - \omega_{sh} \quad (9)$$

where $\omega_{rot} = \frac{1}{2\Im_{rot}}(2I + 1)$ is the core rotational frequency and \Im_{rot} is the core moment of inertia, whose value can be estimated from the slope of the $I(\omega)$ plot for the ground state band (before the neutron alignment). Thus, the parameters for the model for ^{104}Pd can be fixed from the experimental data or the systematics of the mass region.

In the present calculation the configuration for ^{104}Pd was assumed to be $\pi g_{9/2}^{-2} \otimes \nu[h_{11/2}^2, (g_{7/2}/d_{5/2})^2]$ which is the same as for the AMR band of its isotope, namely ^{106}Cd . For this configuration, the symmetric shear is formed between $j_h^{(1)} = j_h^{(2)} = j_\pi = 9/2$ and $j_p = j_\nu = 16$. Since there are eight possible particle - hole and one hole - hole pairs, $n = 8$. Thus, the shear parameters from the calculation of the shear angle and $I(\omega)$ plot were $j = 4.5\hbar$, $a = 3.55$, $V_{\pi\nu} = 1.2$ MeV and $V_{\pi\pi} = 0.2$ MeV. For ^{104}Pd , $I_{sh}^{max} = j_\nu + 9/2 + 7/2 = 24\hbar$ and from experiment $I^{max} = 26\hbar$, which implied that $\Im\omega_{sh}|_{(\theta=0^\circ)} = 2\hbar$. This led to $\Im = 5 \text{ MeV}^{-1}\hbar^2$. \Im_{rot} has been found to be $17 \text{ MeV}^{-1}\hbar^2$ from the slope of the ground state band. With these fixed set of parameters, the numerical values of $I(\omega)$ were calculated and have been shown by the solid line in Fig. 3(b) while the experimental values are shown as filled squares. The calculated values were shifted by the experimental band - head frequency of 0.46 MeV. The comparison plot shows that the numerical values obtained from semi-classical particle rotor model are in good agreement with the experimental values. It is worth noting that in the present model the shears angle (θ) is the only variable and every angular momentum state corresponds to a unique θ . At the band head $\theta = 90^\circ$, $I = j_\nu = 16\hbar$ (from Eq. 5) and $\omega_{sh} = 0$ (from Eq. 7). The high angular momentum states are generated by closing the shears angle and this process has been depicted pictorially in Fig. 4 for ^{104}Pd . The figure shows the shears configuration for the levels of the AMR band which have been characterized by their energy and angular momentum.

The $B(E2)$ values were calculated using Eq. (1) where eQ_{eff} for ^{104}Pd was found to be 1.3 eb from the single particle quadrupole moments of the Nilsson states with Woods-Saxon potential at $\beta_2 = 0.19$ [16]. This prescription has been described in detail in ref. [6]. The shears angle for each state was determined from Eq. (5) and has been given in Fig. 4. The experimental and calculated values have been shown in Fig. 3(a) and the good agreement provided the essential consistency check for the numerical calculations. It is worth noting that though these calculations involved a number of parameters but none of them was left free to obtain the good agreement between the experimental and calculated values.

In summery, the lifetimes of the high spin levels of the yrast cascade of ^{104}Pd have been measured using the DSAM technique. The measured quadrupole transition rates exhibit a monotonically decreasing behaviour with increasing angular momentum in the

domain of $16\hbar \leq I \leq 26\hbar$. In addition, the observed $\mathcal{J}^{(2)}/B(E2)$ values for these levels are large. These feature are definitive indications of AMR. The numerical calculations for AMR based on semi-classical particle rotor model provides a good description of the experimental $I(\omega)$ and $B(E2)$ values. In these calculations, the strengths of particle - hole and hole - hole interactions in ^{104}Pd were assumed to be the same as were found for the Cd isotopes. Thus, AMR has been observed in a nucleus other than Cadmium for the first time which establishes AMR as an alternate mechanism for the generation of high angular momentum states in atomic nuclei.

Authors would like to thank the technical staff of TIFR-BARC pelletron facility for its smooth operation throughout the experiment. The help and cooperation of members of the INGA collaboration for setting up the array are acknowledged. This work was partially funded by the Department of Science and Technology, Government of India (No. IR/S2/PF-03/2003-III). N. R. and P. D. (grant no. PSW-26/11-12) would also like to thank UGC for research support.

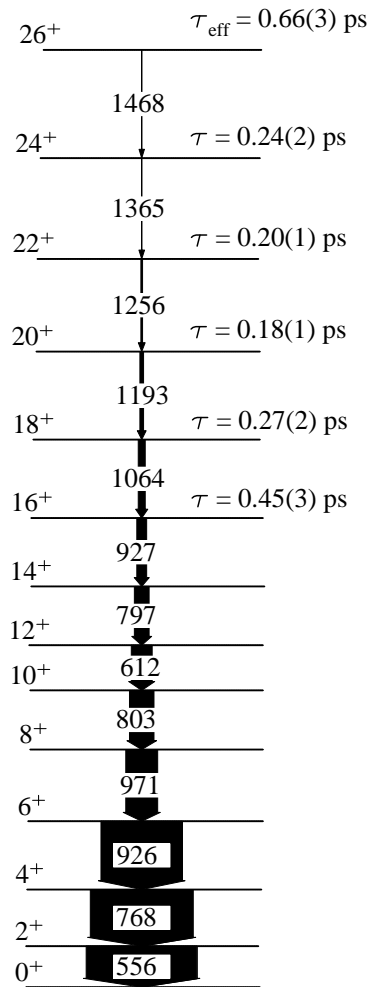


Figure 1: The level structure of the yrast cascade of ^{104}Pd . The energies of the transitions are given in keV and the width of the arrow is proportional to the relative γ -ray intensity.

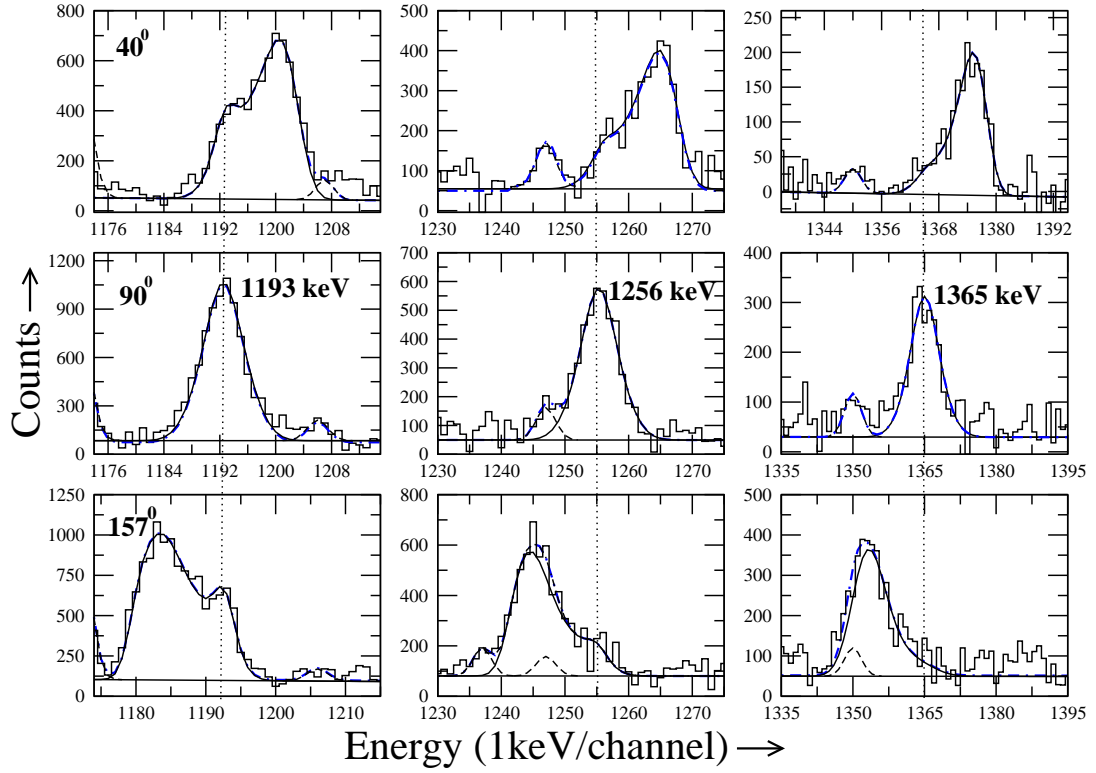


Figure 2: Examples of the lineshape fits for 1193 ($20^+ \rightarrow 18^+$) keV, 1256 ($22^+ \rightarrow 20^+$) keV and 1365 ($24^+ \rightarrow 22^+$) keV transitions at 40° , 90° and 157° with respect to the beam direction. The fitted Doppler broadened lineshapes are drawn in solid lines while the contaminant peaks are shown in dashed lines. The result of the fit to the experimental data is shown in dot-dashed lines.

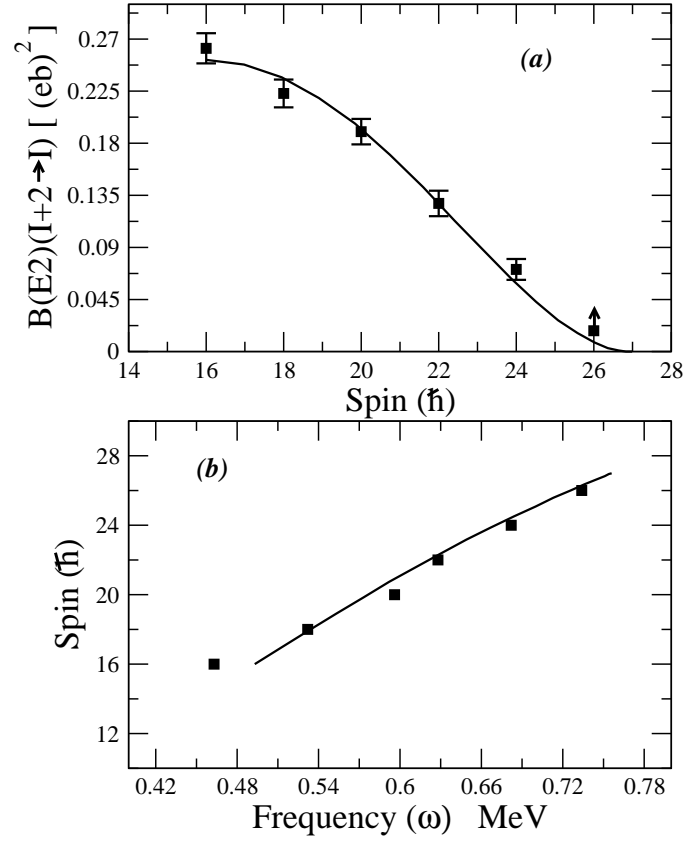


Figure 3: The observed $B(E2)$ rates (a) and the $I(\omega)$ plot (b) in ^{104}Pd . The lines represent the numerical values obtained from the semi-classical particle rotor model for the parameter set as given in the text.

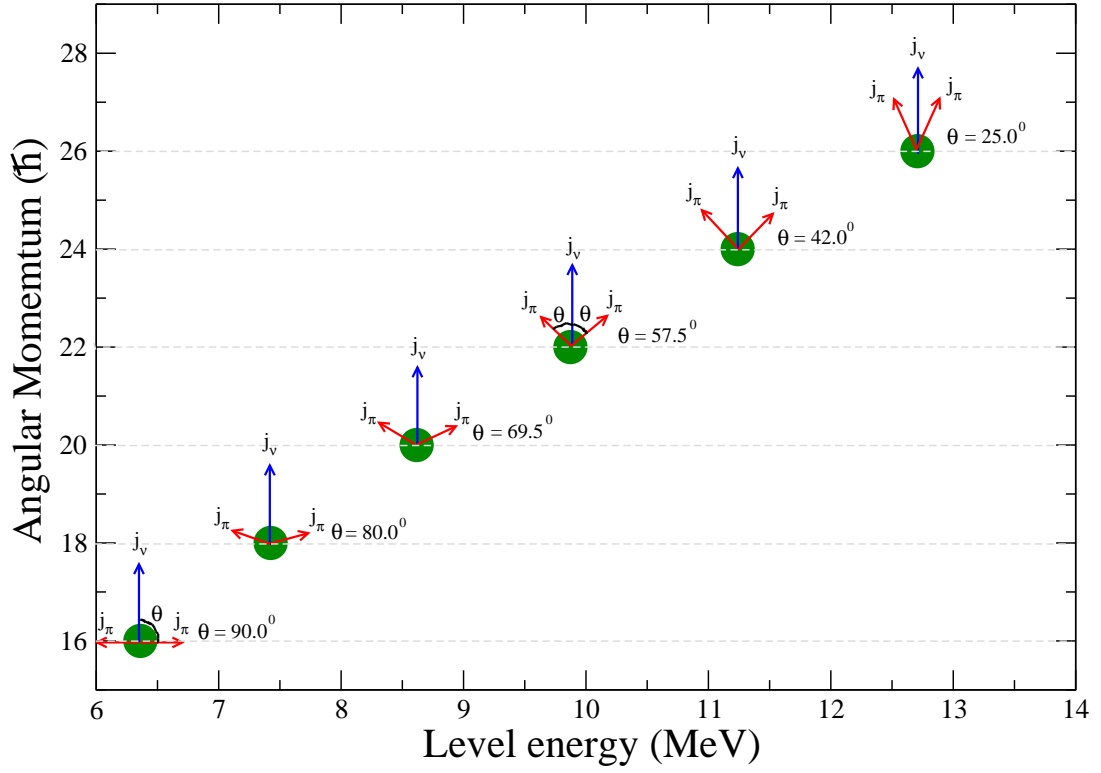


Figure 4: Pictorial representation of symmetric shears structure in ^{104}Pd . The higher spin states are generated by the gradual closing of the shears angle as depicted in the figure.

Spin (\hbar)	Lifetime (ps)	B(E2) (eb) ²	$\mathcal{J}^{(2)}/B(E2)$ [$\hbar^2 MeV^{-1}(eb)^{-2}$]
16 ⁺	0.45 (3)	0.26 (2)	112.3 (8.6)
18 ⁺	0.27 (2)	0.22 (2)	140.9 (12.8)
20 ⁺	0.18 (1)	0.19 (1)	334.2 (17.6)
22 ⁺	0.20 (1)	0.13 (1)	282.3 (21.7)
24 ⁺	0.24 (2)	0.07(1)	554.3 (79.2)
26 ⁺	0.66 (3)	0.02 (1)	

Table 1: The measured lifetimes and the corresponding B(E2) transition rates for high spin yrast cascade of ¹⁰⁴Pd. The last column shows the values of $\mathcal{J}^{(2)}/B(E2)$ ratio.

References

- [1] S. Frauendorf, Nucl. Phys. A 557 (1993) 259.
- [2] S. Frauendorf, Rev. Mod. Phys. 73 (2001) 463.
- [3] R. M. Clark *et al.*, Phys. Rev. Lett. 82, 3220 (1999); P. Datta *et al.*, Phys. Rev. C 69, 044317 (2004); Amita, A. K. Jain and B. Sing, At. Data Nucl. Data Tables 74, 283 (2000). revised edition at [<http://www.nndc.bnl.gov/publications/preprints/mag-dip-rot-bands.pdf>].
- [4] R. M. Clark and A. O. Macchiavelli, Ann. Rev. Nucl. Part. sci. 50, 1 (2000).
- [5] A. J. Simons *et al.*, Phys. Rev. Lett. 91 (2003) 162501.
- [6] P. Datta *et al.*, Phys. Rev. C 71 (2005) 041305(R).
- [7] S. Roy, *et al.*, Phys. Lett. B 694 (2011) 322.
- [8] D. Choudhury *et al.*, Phys. Rev. C 82 (2010) 061308(R); S. Roy and S. Chattopadhyay, Phys. Rev. C 87 (2013) 059801.
- [9] D. Choudhury *et al.*, Phys. Rev. C 87 (2013) 034304(R).
- [10] S. Zhu *et al.* Phys. Rev C 64 (2001) 041302 (R).
- [11] M. Sugawara *et al.*, Phys. Rev C 86 (2012) 034326.
- [12] M. Sugawara *et al.*, Phys. Rev. C 79 (2009) 064321.
- [13] S. Muralithar, *et al.*, Nucl. Instrum. Methods A 622 (2010) 281.
- [14] R. Palit, *et al.*, Nucl. Instrum. Methods A 680 (2012) 90.
- [15] D. C. Radford, Nucl. Instrum. Methods, A 361 (1995) 297.
- [16] D. Sohler, *et al.*, Phys. Rev. C 85, (2012) 044303.
- [17] J. C. Wells and N. R. Johnson, Oak Ridge National Laboratory Report No. ORNL-6689, (1991) 44.
- [18] L. C. Northcliffe, *et al.*, Nucl. Data, Sect. A7, (1970) 233.
- [19] F. James *et al.*, Comput. Phys. Commun. 10, (1975) 343.
- [20] B. A. Brown *et al.*, Phys. Rev. C 9, (1974) 1033.
- [21] S. Roy and S. Chattopadhyay, Phys. Rev. C 83 (2011) 024305.